"This document is the unedited Author's version of a Submitted Work that was subsequently accepted for publication in Nano Letters, copyright © American Chemical Society after peer review. To access the final edited and published work see http://pubs.acs.org/doi/abs/10.1021/nl102259s."

NANO LETTERS

pubs.acs.org/NanoLett

Directed Self-Assembly at the 10 nm Scale by Using Capillary Force-Induced Nanocohesion

Huigao Duan,[†,‡] and Karl K. Berggren[†,*]

[†]Department of Electrical Engineering and Computer Science, Massachusetts Institute of Technology, Cambridge, Massachusetts 02139 and [‡]School of Physical Science and Technology, Lanzhou University, Lanzhou, Gansu 730000, People's Republic of China

ABSTRACT We demonstrated a new nanoassembly strategy based on capillary force-induced cohesion of high-aspect ratio nanostructures made by electron-beam lithography. Using this strategy, ordered complex pattern were fabricated from individual nanostructures at the 10 nm length scale. This method enables the formation of complex designed networks from a sparse array of nanostructures, suggesting a number of potential applications in fabrication of nanodevices, nanopatterning, and fluid-flow investigations.

KEYWORDS Capillary force, self-assembly, nanocohesion, electron-beam lithography, 10-nm-scale

Capillary force plays a dominant role in a large range of natural phenomena[1−8] and has been widely used as a driving force for the self-assembly of nanoscale to mesoscale objects.[9−18] However, these self-assembly processes based on capillary forces were limited to the microscale and mesoscale and have never been used in patterning sub-100 nm length-scale structures. Furthermore, local control of self-assembly on this length scale had not been achieved. In this report, we demonstrate a directed-assembly process based on controllable capillary force-induced nanocohesion that can precisely assemble individual high-aspect ratio structures at 10 nm length scales into complex hierarchical structures.

The basic idea of this nanoassembly process is shown in Figure 1a, where straight high-aspect ratio nanopillars are first defined as latent features in resist and then developed in a liquid developing agent. In the subsequent drying process, capillary force exists between the nanopillars on the nanopillar liquid−air interface.[2,19] When the capillary force is larger than a critical force,[19,20] the nanopillars will collapse, potentially resulting in nanocohesion. If the adhesion force between the cohered pillars (or between the pillars and the substrate) is larger than the elastic force acting to restore the pillars to their original shape, the cohesion would be sustained after drying. By adjusting the spatial distribution of nanopillars, this cohesion can be used to form complex two-dimensional structures at the 10 nm length scale.

An example of this process is shown in Figure 1b,c where we fabricated two arrays of uniformly distributed high-aspect ratio negative poly(methyl methacrylate) (PMMA) nanopillars[21] using the same parameters but dried one of them by using a supercritical-point carbon dioxide dryer (for Figure 1b) and the other by using a spin dryer (for Figure 1c). The diameter of the pillars was ∼15 nm, the height was ∼80 nm, and the pitch was 50 nm. In Figure 1b, all of the high-aspect ratio nanopillars remained standing because the supercritical-point drying process eliminated the surface tension and resultant capillary force; while in Figure 1c, all of the pillars collapsed and cohered into various assemblies because of the capillary force induced in the liquid-evaporation process.

Similar capillary force-induced collapse effects have been widely reported as unwanted random behaviors in many high-aspect ratio structures such as carbon nanotubes,[22] ZnO nanowires,[23] silicon nanorods,[24] polymer micropillars,[25] and general resist structures.[8,26] In these cases, the random collapse is thought to result from the combination of many factors[27] such as capillarity, self-weight,[28] anisotropic geometry,[29] and even a domino effect.[18,30] To direct the collapse, we must use one of these factors as the main driving force. Recently, domino effect-based,[30] gel-assisted,[31] and asymmetric geometry-based[29] self-organizations of nanopillars or microneedles have been reported. However, these self-organization processes still cannot be well controlled or designed to achieve arbitrary two- or three-dimensional nanostructures.

In this work, we used intentionally asymmetric capillary forces to reproducibly direct the self-assembly of nanopillars to form ordered, designable nanostructures. Comparing to previous work, our study focused on how to deterministically control the capillary force-induced self-assembly of high-aspect ratio structures at 10-nm-length scales. By locally varying the initial relative positions in the top-down nanofabrication process and by tuning the critical minimum cohesion force of structures by using electron-exposure dose, complex, predesigned and defect-free hierarchical patterns were deterministically self-assembled from sparse individual posts.

---

[*] To whom correspondence should be addressed. E-mail: berggren@mit.edu.

Received for review: 06/28/2010
Published on Web: 08/12/2010

DOI: 10.1021/nl102259s | *Nano Lett.* **2010,** *10,* 3710–3716

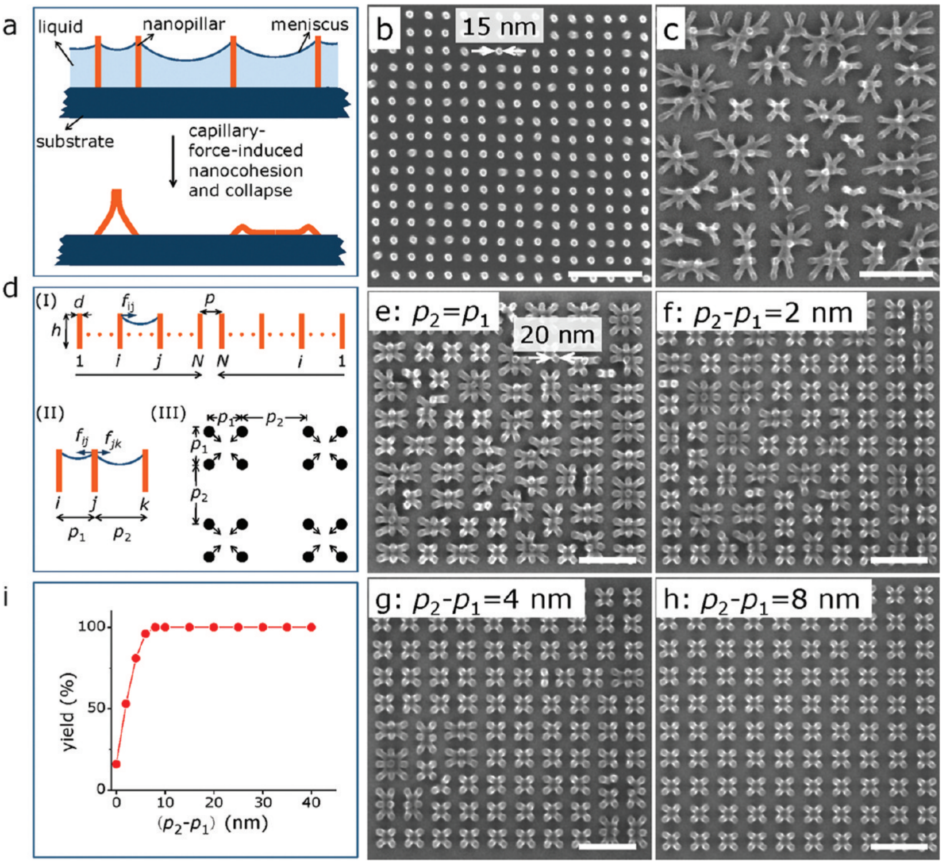

FIGURE 1. Schematics of controllable capillary force-induced nanocohesion process. (a) Schematic of nanoassembly by capillary force-induced cohesion of high-aspect ratio nanostructures in the drying process. (b) Scanning-electron microscopy (SEM) image of 50 nm pitch nanopillars with diameter ~15 nm fabricated by electron beam lithography using PMMA as a negative resist. The thickness of PMMA was ~90 nm, the lithographic electron dose for each individual pillar was 300 fC, and the resultant height of nanopillars was ~80 nm. The sample was developed by 1:2 methyl isobutyl ketone−IPA for 1 min at 20 °C, rinsed by pure IPA, and then dried in a supercritical point dryer. (c) SEM image of negative PMMA nanopillars dried in a spin dryer in air at room temperature in which pattern collapse was induced by capillary forces in the liquid-evaporation process. The nanopillars were fabricated by using the same parameters as those in (b). (d) Schematic of (I) a one-dimensional uniform $2N$-nanopillar array, (II) 3-pillar array, and (III) a two-dimensional nanopillar array with designed capillary force to direct the pattern collapse. In (III), p_1 is the pitch of nanopillars in the same cell and p_2 is defined as the intercell spacing of two adjacent cells. When $p_2 \neq p_1$, asymmetric capillary forces will be introduced. (e−h) SEM images of cohered nanopillars with $p_2 = p_1$ (e), $p_2 - p_1 = 2$ nm (f), $p_2 - p_1 = 4$ nm (g), $p_2 - p_1 = 8$ nm (h), demonstrating that the yield of deterministic cohesion increased when increasing intercell spacing p_2. The diameter of nanopillars was ~20 nm, the pitch of pillars in the cell p_1 was 50 nm, and the lithographic electron dose for each individual pillar was 400 fC. (i) Quantitative yield as a function of the value of intercell spacing variation ($p_2 - p_1$), which shows high yield of deterministic cohesion when ($p_2 - p_1$) was large enough. All SEM images show the full extent of the patterned region, and their scale bars are 200 nm.

The capillary force between two pillars i and j is given by

$$f_{ij} = 2\pi S_{ij}\gamma \cos \alpha / p_{ij} \tag{1}$$

where S_{ij} is the effective surface area contributing to capillary force, γ is the surface tension of liquid, α is the contact angle between liquid and the pillars, and p_{ij} is the distance between pillars i and j prior to collapse.[32] The net force on an individual pillar i in a pillar array is the sum of capillary forces from all other pillars.

To simplify the description, we consider the situation shown in Figure 1d (I) of a one-dimensional uniform symmetric series of $2N$ pillars (for odd numbers of pillars, the capillary force for the middle pillar is zero due to symmetry). In this case, the total capillary force for the pillar i is given by

$$f_i = 2\pi\gamma \cos \alpha \sum_{j=1,\neq i}^{2N} S_{ij}\frac{1}{(j-i)p}(1 \leq i \leq \mathrm{N}, 1 \leq j \leq 2N) \tag{2}$$

where p is the pitch of this pillar array (because the pillars are generally much smaller in diameter than the spacing between them, we assumed that the diameter of the pillar can be neglected when determining the distance of pillars for the calculation of capillary force), S_{ij} can be considered as the effective surface area contributing to capillary force between pillars i and j, which decreases when increasing the distance between pillars i and j.

Because of the symmetry of the system, many terms cancel out and we can simplify eq 2 to get the asymmetric capillary force for each pillar

$$f_i = 2\pi\gamma \cos\alpha \sum_{j=2i}^{2N} S_{ij}\frac{1}{(j-i)p}(1 \leq i \leq N, 1 \leq j \leq 2N) \tag{3}$$

From this equation, we know that, for a fixed pillar-number $2N$, boundary pillars ($i = 1$) have the largest asymmetric capillary force, and the asymmetric capillary force applied on the pillar i decreases when it is closer to the middle (i.e., increasing i to N), while the central pillars have the smallest asymmetric capillary force ($i = N$). There exists a critical minimum lateral force $f_{\min}$ to collapse a pillar.[19,20] When $f_i > f_{\min}$, the pillar i will collapse in the direction of the capillary force; when $f_i < f_{\min}$, the pillar i will remain vertical. Thus the pillars closer to the boundary prefer to collapse toward the center, while the pillars closer to the middle prefer to stand. In an ideal infinitely uniform pillar array, no pillar will collapse because the capillary forces for any pillar equilibrate to zero. In reality, there exist other random facts such as pillar displacement, intrinsic imperfections of pillars, and the dynamics of dewetting, which could introduce random deformation or collapse of some pillars. In particular, these initial random deformations or collapses could break the symmetry of the surroundings and induce dynamic effects.

The scenario shown in Figure 1c can thus be understood to be determined by the combined effects described above, in which boundary pillars had enough asymmetric capillary force toward the center of the array, so they collapsed to the center, but inner pillars collapsed randomly because the directed capillary forces were insufficient and thus their collapse was determined by random effects.

To direct collapse of all pillars, the asymmetric capillary force f_i of all the pillars must be larger than $f_{\min}$. There are two possible ways to achieve this result: (1) by increasing asymmetric capillary force for all pillars; and (2) by decreasing the minimum critical collapse force $f_{\min}$. We will discuss each of these possible approaches.

To demonstrate control and strengthening of the asymmetric capillary force, we introduced asymmetric design in a pillar array to achieve designed force on all pillars. The schematic of our simplest method is shown in Figure 1d (II), where the capillary force of the center pillar is

$$\begin{aligned} f_j = f_{ij} - f_{jk} = 2\pi S\gamma \cos\alpha/p_1 - \\ 2\pi S\gamma \cos\alpha/p_2 \sim (1/p_1 - 1/p_2) = (p_2 - p_1)/p_1p_2 \end{aligned} \tag{4}$$

When the pitch difference of $p_2 - p_1$ is much smaller than p_1p_2, $f_j \propto (p_2 - p_1)$, implying that the asymmetric capillary force increases with increasing the pitch difference. When the designed asymmetric capillary force f_j is large enough to overcome all other random effects, the collapse is directed.

This concept can be extended to a two-dimensional array of pillars. We designed a periodic two-dimensional 4-pillar-unitcell array of nanopillars, as shown in Figure 1d (III). We fixed the intracell pitch p_1 and varied the intercell spacing p_2. When p_2 was greater than p_1, the asymmetric capillary force of each pillar pointed to the center of its cell. We patterned an array of nanopillars in PMMA using a negative-tone electron-beam lithography (EBL) process. After development in developer and rinsing in isopropyl alcohol (IPA), the negative PMMA nanopillars were spin-dried. The intracell pitch p_1 was 50 nm, the pillars were ~80 nm tall, and the diameter was ~20 nm. The intercell spacing p_2 varied from 50 to 90 nm.

In the case of $p_2 = p_1$ shown in Figure 1e, the pillars collapsed randomly and formed different assemblies consisting of between 2 and 9 elements. As p_2 increased, the yield of the intended intracell 4-pillar collapse increased correspondingly (Figure 1f,g), indicating that the collapse of the pillars were more directed and controllable. Once p_2 was large enough, the yield reached 100%, as shown in Figure 1h, where $(p_2 - p_1)$ was 8 nm, that is, a 16% increase relative to the intracell pitch p_1. The yield as a function of $(p_2 - p_1)$ is shown in Figure 1i from which we can see a clear systematic trend.

To further demonstrate the reliability of this strategy, we designed a series of multielement cells with different cell geometries. Figure 2a,f shows that assemblies with 2, 3, 4, 6, 7, and 9 elements in each cell nanocohered as designed, where the intercell spacing p_2 was ~2 times that of the intracell pitch p_1, and all other parameters were the same as those in Figure 1e,h. In these assemblies, we can see that all boundary pillars in any single cell cohered to the center of the cell rigidly, while the middle pillars (in 7- and 9-element cell, shown in Figure 2e,f, respectively) remained vertical because of symmetry within the cell. No imperfections were found across ~16 μm^2 patterns (400 cells, our largest test area for this sample).

Figure 2g shows a new type of example in which 9-pillar-cell arrays with 4 different rotations were self-assembled, from which we can see robustly ordered assemblies were achieved by capillary force-induced nanocohesion. This nanocohesion-based self-assembly could also be achieved across a range of length scales with different materials and geometries (Supporting Information Figure S1−S3).

Though we could get robust ordered assemblies for small-element number cells because the asymmetric capillary force was large enough to direct cohesion for all pillars, the assembly of larger-element number (>25) uniform cells was more difficult (Figure 1c and Supporting Information Figure S4) because the lower asymmetric capillary force for inner

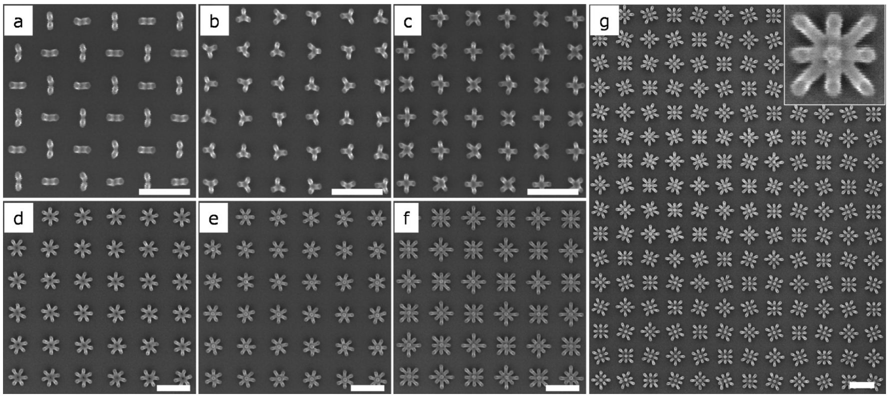

FIGURE 2. SEM images of ordered multielement assemblies fabricated by capillary force-induced nanocohesion. (a) A 2-element-cell with two different rotations; (b) 3-element-cell with three different rotations; (c) 4-element-cell with two different rotations; (d) 6-element-cell with three different rotations; (e) 7-element-cell with three different rotations; (f) 9-element-cell with two different rotations; and (g) large area 9-element-cell with four different rotations. The diameter of nanopillars was ∼20 nm, the pitch of pillars in the cell was 50 nm, and the intercell spacing between adjacent cells was ∼100 nm. The thickness of PMMA was ∼90 nm and the resultant negative PMMA nanopillars were ∼80 nm tall. All scale bars are 200 nm.

pillars permitted random collapse. For this case, we describe here that directed self-assembly could still be realized by controlling the critical minimum cohesion force $f_{\min}$ through varying the dot exposure dose during the lithography process (and thus varying the pillar diameter and perhaps also slightly varying its intrinsic strength).

For a pillar in an array with a given pitch, the critical minimum cohesion force[33] is given by

$$f_{\min} \sim Ed^4/h^3 = Ed/A^3 = Eh/A^4 \qquad (5)$$

where E is Young's modulus, d is the diameter of the pillar, h is the height of the pillar, and A is the aspect ratio of the pillar defined by $A = h/d$. This formula implies that to decrease $f_{\min}$, we can increase the elasticity (i.e., decrease E), decrease the diameter d, or increase the height h. When elasticity variation is negligible, increasing aspect ratio A is the most effective way to decrease $f_{\min}$.

To engineer $f_{\min}$, we fabricated a uniform 171-element array of hexagonal high-aspect ratio negative PMMA nanopillars. The height of the pillars h was ∼550 nm, and the pitch p was 200 nm. The diameter d of pillars was controlled by changing the exposure dose of each pillar, which allowed us to achieve varying aspect ratios. Figure 3a−d shows the evolution of nanocohesion of this 171-element nanopillar array as the aspect ratio was increased by decreasing lithographic electron exposure. From these figures, we can see that with decreasing pillar diameter, pillars tended to cohere toward the pattern center.

We can use the theoretical picture described above to give a qualitative explanation of the dynamic process of each scenario. To illustrate the process, we consider a uniformly spaced one-dimensional 8-nanopillar array, shown schematically in Figure 3a′−d′, in which the initial asymmetric capillary forces for each nanopillar are f_1, f_2, f_3, and f_4, and $f_1 > f_2 > f_3 > f_4$ according to our model. Suppose the critical minimum lateral cohesion forces for each of the pillars in Figure 3a−d were f_a to f_d. With decreasing the diameter, from formula 5, we know $f_a > f_b > f_c > f_d$. In the first case (Figure 3a), we believe the initial condition was $f_1 > f_a > f_2 > f_3 > f_4$, so pillar 1 collapsed first. During the collapse of pillar 1, the distance between pillar 1 and pillar 2 decreased and the capillary force between them increased dramatically ($f \sim 1/p_{12}$), which made f_2 reverse in directions and increase in magnitude so that it induced pillar 2 to collapse toward pillar 1 (we describe this dynamic interaction as a "domino effect"); after pillar 2 collapsed, the asymmetric capillary forces for pillar 3 and pillar 4 increased but were still smaller than the critical force f_a required to induce the collapse (Figure 3a′). In the second case (Figure 3b), the initial condition was also $f_1 > f_b > f_2 > f_3 > f_4$, so that pillar 1 collapsed and induced pillar 2 collapse toward pillar 1 as in the first case. However, in contrast to the first case, during the collapse process of pillar 2, the asymmetric capillary force for pillar 3 was now sufficient to collapse pillar 3 toward pillar 4, and another domino effect took place for the remaining pillars (Figure 3b′). In the third case (Figure 3c), we understand $f_1 > f_2 > f_3 > f_c > f_4$, so pillar 1, 2, and 3 initially collapsed to the center and induced pillar 4 to collapse to pillar 3 (Figure 3c′). In the last case (Figure 3d), the initial asymmetric capillary force of all pillars was such that $f_1 > f_2 > f_3 > f_4 > f_d$, so that all of them collapsed to the center (Figure 3d′). The above-mentioned dynamic processes were also found in nonuniform pillar arrays, shown in Supporting Information Figure S5.

More symmetric assemblies could be obtained from smaller arrays, as shown in Figure 3e and Supporting Information Figure S6, where hexagonal nanopillar arrarys were assembled into symmetric nanohills. This symmetry was possible because the asymmetric capillary force for the pillar nearest to the middle should be $f_N \sim 1/Np$ according

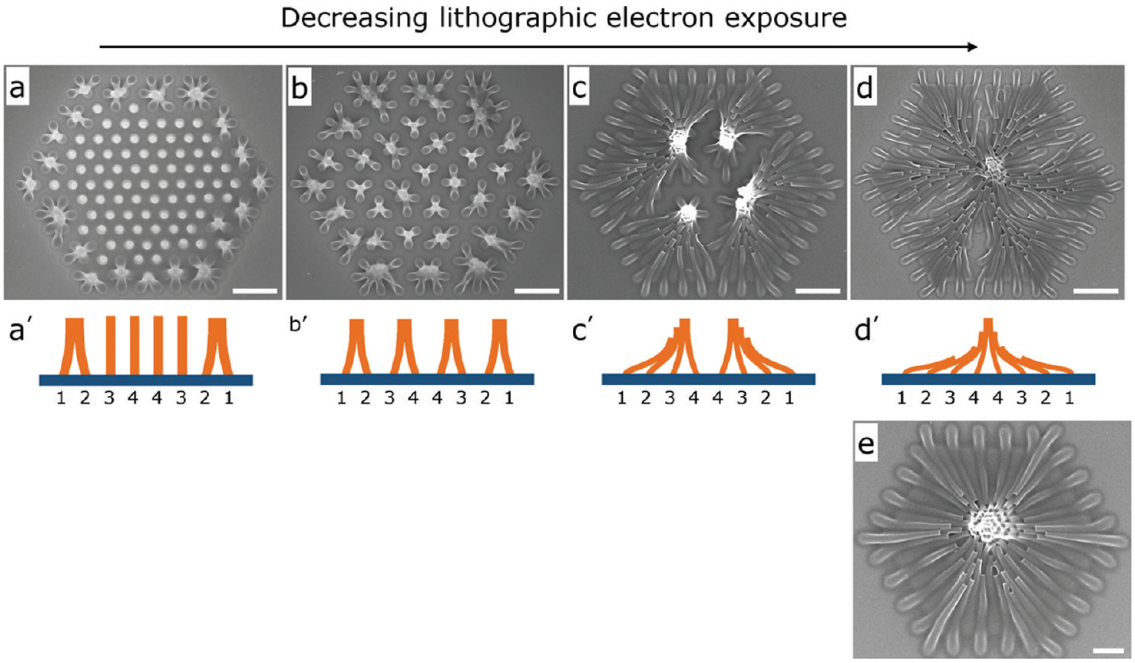

FIGURE 3. SEM images of large-element-number assemblies fabricated by capillary force-induced nanocohesion. (a−d) SEM images of the evolution of a 171-pillar array with increasing the aspect ratio by decreasing lithographic electron exposure dose: (a) 5.7, (b) 4.0, (c) 2.8, and (d) 2.0 pC/pillar, showing how asymmetric capillary force determined nanocohesion of a large array with different aspect ratios. The pitch of the pillars was 200 nm. The scale bars are 500 nm. (a′−d′) Cross-sectional schematic diagrams of different scenarios for (a−d). (e) SEM image of a symmetric nanohill collapsed from a 91-pillar array (smaller than in cases a−d) with a pitch of 160 nm by nanocohesion. Scale bar is 200 nm. The PMMA thickness was ∼600 nm and resultant height of nanopillars was ∼550 nm.

to eq 3, so for fewer-element pillar arrays, pillars closer to the middle should be more easily directed compared to larger arrays. We also noticed that although increasing the aspect ratio could increase the fidelity of self-assembly, the collapse of nanopillars would be partly determined by random effects when the aspect ratio was too high, resulting in random collapse of some pillars (see Supporting Information Figure S7). In this case, we believe that the critical lateral collapse force $f_{\min}$ was so small that it was comparable with random forces induced by imperfections and self-weight of pillars, so random forces partly affected the collapse.

As described above, the action of nanocohesion was determined by the relationship of designed asymmetric capillary force and the critical collapse force $f_{\min}$ of nanopillars. By deliberately setting this relationship for all the nanopillars in a pattern, we also showed that complex hierarchical nanostructures could be fabricated by nanocohesion as is evident in Figure 4.

Figure 4a shows some hierarchical designs where the basic concept was to deliberately vary the local position (by ∼10%, relative to a uniform distribution) of some pillars in a larger cell to create controlled substructures. Thus, while boundary pillars in the cell had the largest capillary force, the pillars in the designed substructures also had sufficient capillary forces to induce directed collapse, as shown schematically by the arrows in Figure 4a. Figure 4b shows complex hierarchical networks fabricated on the basis of the designs in Figure 4a, from which we can see that the pillars collapsed and self-assembled in the expected directions to form the desired patterns. Though the yield decreased when increasing the total element-number in these tests, we believe this technique could be further improved by optimizing the pillar placement and geometry.

The central result of this report is the demonstration of a new nanoassembly strategy based on capillary force-induced cohesion of high-aspect ratio nanostructures during the postdevelopment drying process. By using this strategy, robust ordered complex networks of nanostructures were fabricated. Though we focused here on patterning with electron beam lithography, we believe that this technique can be also applied to other high-aspect ratio nanostructures, including functional vertically aligned semiconductor nanowires or nanorods, carbon nanotubes, or metal nanopillars to perhaps permit functional self-assembled structures. On the other hand, from a lithographer's point of view, this self-assembly technique suggests a number of potential applications in electron-beam lithography, including (1) increasing the throughput by patterning only a portion of the final structures, then increasing the pattern area by inducing controlled collapse; (2) reducing proximity effect[34] by reducing the total dose needed to make patterns in a given area (again by patterning only pillars, then inducing collapse to make linear structures); and (3) reducing electron exposure in radiation-sensitive devices by using induced collapse across sensitive device material to define a device feature. One limitation of this method is that accurate pattern

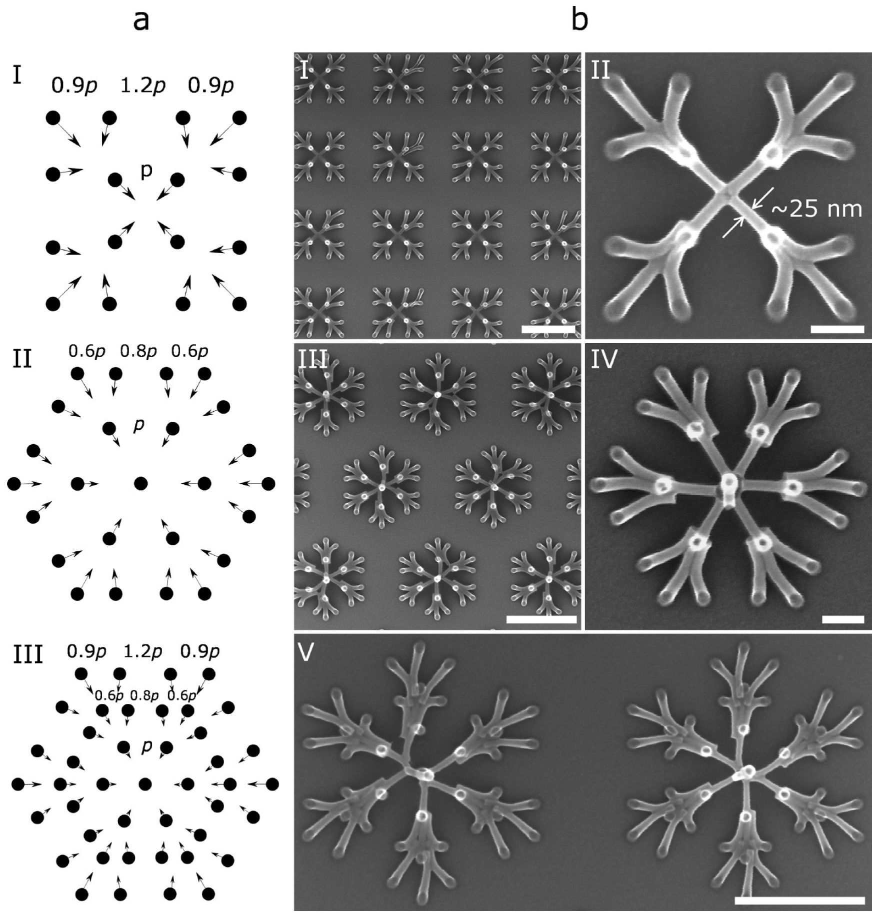

FIGURE 4. SEM images of hierarchical assemblies fabricated by capillary force-induced nanocohesion. (a) Schematics of simple hierarchical designs using 16 (I), 25 (II), and 43 (III) pillars. (b) SEM images of symmetric hierarchical networks collapsed from the designs in (a), with p value of 150 nm. The scale bars for b (I, III, V) are 500 nm, for b (II and IV) are 100 nm. The diameter of PMMA nanopillars was ~25 nm. The thickness of PMMA here was ~250 nm and the resultant height of nanopillars was ~220 nm.

transfer of collapsed structures to functional layers may be challenging because the sidewall profile of collapsed structures is not vertical, and the diameter of electron beam lithography-defined high-aspect ratio structures may not be perfectly uniform along their length (due to forward scattering of exposing electrons). More work should be done in the future to apply this method for fabricating functional devices. Finally, because the process can take place at sub-20 nm scale, this technique could also serve as a platform for scientific investigation of fluid flow near the molecular scale to study the mechanism of evaporation, dewetting phenomena, and the mechanical behaviors of structures on the 10-nm length scale.

Acknowledgment. This work was supported by Office of Naval Research and Nanoelectronics Research Initiative. Patterning was done at MIT's shared scanning-electron-beam-lithography facility in the Research Laboratory of Electronics. We thank M. Mondol and J. Daley for technical assistance and Dr. Joel Yang for helpful discussion. H. G. Duan was supported by a fellowship from the China Scholarship Council.

Supporting Information Available. Methods, additional figures, and additional references. This material is available free of charge via the Internet at http://pubs.acs.org.

REFERENCES AND NOTES

(1) de Gennes, P. G.; Brochard-Wyard, F.; Quere, D. *Capillarity and Wetting Phenomena: Drops, Bubbles, Pearls, Waves*; Springer: New York, **2003**.
(2) Bico, J.; Roman, B.; Moulin, L.; Boudaoud, A. *Nature* **2004**, *432*, 690.
(3) Kim, H. Y.; Mahadevan, L. *J. Fluid Mech.* **2006**, *548*, 141–150.
(4) Gao, X. F.; Jiang, L. *Nature* **2004**, *432*, 36.
(5) Geim, A. K.; Dubonos, S. V.; Grigorieva, I. V.; Nonoselov, K. S.; Zhukov, A. A.; Shapoval, S. Yu. *Nat. Mater.* **2003**, *2*, 461–463.
(6) Blossey, R. *Nat. Mater.* **2003**, *2*, 301–306.
(7) Guo, J. G.; Zhou, L. J.; Zhao, Y. P. *J. Colloid Interface Sci.* **2009**, *331*, 458–462.
(8) Ahn, M.; Heilmann, R. K.; Schattenburg, M. L. *J. Vac. Sci. Technol., B* **2007**, *25*, 2593–2597.
(9) Yin, Y. D.; Lu, Y.; Gates, B.; Xia, Y. N. *J. Am. Chem. Soc.* **2001**, *123*, 8718–8729.
(10) Kraus, T.; Malaquin, L.; Schmid, H.; Riess, W.; Spencer, N. D.; Wolf, H. *Nat. Nanotechnol.* **2007**, *2*, 570–576.
(11) Peyrade, D.; Gordon, M.; Hyvert, G.; Berton, K.; Tallal, J. *Microelectron. Eng.* **2006**, *83*, 1521–1525.
(12) Cui, Y.; Björk, M. T.; Liddle, J. A.; Sönnichsen, C.; Boussert, B.; Alivisatos, A. P. *Nano Lett.* **2004**, *4*, 1093–1098.

(13) Rothemund, P. W. *Proc. Natl. Acad. Sci. U.S.A.* **2000**, *97*, 984–989.

(14) Bowden, N.; Terfort, A.; Carbeck, J.; Whitesides, G. M. *Science* **1997**, *276*, 233–235.

(15) Py, C.; Reverdy, P.; Doppler, L.; Bico, J.; Roman, B.; Baroud, C. N. *Phys. Rev. Lett.* **2007**, *98*, 156103.

(16) Guo, X. Y.; Li, H.; Ahn, B. Y.; Duoss, E. B.; Hsia, K. J.; Lewis, J. A. *Proc. Natl. Acad. Sci. U.S.A.* **2009**, *106*, 20149–20154.

(17) Jacobs, H. O.; Tao, A. R.; Schwartz, A.; Gracias, D. H.; Whitesides, G. M. *Science* **2002**, *296*, 323–325.

(18) Pokroy, B.; Kang, S. H.; Mahadevan, L.; Aizenberg, J. *Science* **2009**, *323*, 237–240.

(19) Cohen, A. E.; Mahadevan, L. *Proc. Natl. Acad. Sci. U.S.A.* **2003**, *100*, 12141–12146.

(20) Neukirch, S.; Roman, B.; de Gaudemaris, B.; Bico, J. *J. Mech. Phys. Solids* **2007**, *55*, 1212–1235.

(21) Duan, H. G.; Zhao, J. G.; Zhang, Y. Z.; Xie, E. Q.; Han, L. *Nanotechnology* **2009**, *20*, 135306.

(22) Lau, K. K. S.; et al. *Nano Lett.* **2003**, *3*, 1701–1705.

(23) Dev, A.; Chaudhuri, S. *Nanotechnology* **2007**, *18*, 175607.

(24) Zhao, Y. P.; Fan, J. G. *Appl. Phys. Lett.* **2006**, *88*, 103123.

(25) Chandra, D.; Yang, S.; Soshinsky, A. A.; Gambogi, R. J. *Appl. Mater. Interfaces* **2009**, *1*, 1698–1704.

(26) Tanaka, T.; Morigami, M.; Atoda, N. *Jpn. J. Appl. Phys.* **1993**, *32*, 6059–6064.

(27) Zhang, Y.; Lo, C. W.; Taylor, J. A.; Yang, S. *Langmuir* **2006**, *22*, 8595–8601.

(28) Hui, C. Y.; Jagota, A.; Lin, Y. Y.; Karmer, E. J. *Langmuir* **2002**, *18*, 1394–1407.

(29) Pokroy, B.; Epstein, A. K.; Persson-Gulda, M. C. M.; Aizenberg, J. *Adv. Mater.* **2009**, *21*, 463–469.

(30) Wu, D.; Chen, Q. D.; Xu, B. B.; Jiao, J.; Xu, Y.; Xia, H.; Sun, H. B. *Appl. Phys. Lett.* **2009**, *95*, No. 091902.

(31) Sidorenko, A.; Krupenkin, T.; Taylor, A.; Fratzl, P.; Aizenberg, J. *Science* **2007**, *315*, 487–490.

(32) Israelachvili, J. N. *Intermolecular and Surface Forces*, 2nd ed.; Academic Press Ltd.: London, 1992.

(33) Beer, F. B.; Johnston, E. R. *Mechanics of Materials*, 2nd ed.; McGraw-Hill: New York, 1992.

(34) Chang, T. H. P. *J. Vac. Sci. Technol.* **1975**, *12*, 1271–1275.